Proc. Natl. Acad. Sci. USA
Vol. 92, pp. 11220–11224, November 1995
Biophysics

Membrane transport mechanisms probed by capacitance measurements with megahertz voltage clamp

CHIN-CHIH LU*, ANATOLII KABAKOV*, VLADISLAV S. MARKIN†, SELA MAGER‡, GARY A. FRAZIER§, AND DONALD W. HILGEMANN*¶

Departments of *Physiology and †Cell Biology, University of Texas Southwestern Medical Center, 5323 Harry Hines Boulevard, Dallas, TX 75235; ‡Division of Biology, California Institute of Technology, Pasadena, CA 91125; and §Texas Instruments, Inc., Dallas, TX 75275

Communicated by A. J. Hudspeth, University of Texas Southwestern Medical Center, Dallas, TX, August 10, 1995
(received for review March 8, 1995)

ABSTRACT **We have used capacitance measurements with a 1-μs voltage clamp technique to probe electrogenic ion–transporter interactions in giant excised membrane patches. The hydrophobic ion dipicrylamine was used to test model predictions for a simple charge-moving reaction. The voltage and frequency dependencies of the apparent dipicrylamine-induced capacitance, monitored by 1-mV sinusoidal perturbations, correspond to single charges moving across 76% of the membrane field at a rate of 9500 s^{-1} at 0 mV. For the cardiac Na,K pump, the combined presence of cytoplasmic ATP and sodium induces an increase of apparent membrane capacitance which requires the presence of extracellular sodium. The dependencies of capacitance changes on frequency, voltage, ATP, and sodium verify that phosphorylation enables a slow, 300- to 900-s^{-1}, pump transition (the E_1–E_2 conformational change), which in turn enables fast, electrogenic, extracellular sodium binding reactions. For the GAT1 (γ-aminobutyric acid,Na,Cl) cotransporter, expressed in *Xenopus* oocyte membrane, we find that chloride binding from the cytoplasmic side, and probably sodium binding from the extracellular side, results in a decrease of membrane capacitance monitored with 1- to 50-kHz perturbation frequencies. Evidently, ion binding by the GAT1 transporter suppresses an intrinsic fast charge movement which may originate from a mobility of charged residues of the transporter binding sites. The results demonstrate that fast capacitance measurements can provide new insight into electrogenic processes closely associated with ion binding by membrane transporters.**

The development of structure–function models of membrane transporters (1) requires not only high-resolution structural information (e.g., see refs. 2 and 3) but also detailed functional information (4), which is available for only a few transporters to date. Studies of the electrogenic reactions of a transporter—i.e., those reactions which move net charges with respect to membrane electrical field—can provide important insights into transport mechanisms and kinetics (4–8). To identify such reactions, they must be isolated experimentally and be shown to generate electrical current (or charge movements), influence membrane potential, and/or be sensitive to changes of membrane potential.

The implementation of fast capacitance (admittance) measurements was suggested by recent studies of the Na,K pump (8, 9). Briefly, extracellular binding of Na^+ by the Na,K pump was associated with charge movements which were complete within 4 μs (9). On this basis, changes of sodium binding site availability should result in significant changes of the apparent membrane capacitance (i.e., charge stored per unit change of membrane potential), and similar considerations apply equally to other electrogenic reactions. Similarly, it has been proposed for the Na,Ca–K exchanger of the rod outer segment (10), the Na/glucose cotransporter (11), the cardiac Na,Ca exchanger (12), and the GAT1 [Na,γ-aminobutyric acid (GABA),Cl] cotransporter (13) that extracellular sodium binding reactions are the major electrogenic reactions.

MATERIALS AND METHODS

Giant Excised Patches. Giant membrane patches (14, 15) were formed from guinea pig cardiac myocytes and *Xenopus* oocytes (>1-GΩ seals; 6- to 12-pF membrane capacitance). To avoid capacitance changes with solution level changes, pipette tips were thickly coated with a highly viscous Parafilm/mineral oil mixture (for details, see ref. 14).

Capacitance (Admittance) Measurements. For current resolution up to 50 kHz, Axopatch 1C and 200A amplifiers were employed. Membrane capacitance changes were monitored as admittance changes by Princeton lock-in amplifiers (5302 and 5209) using sinusoidal voltage perturbations of 0.5–2 mV at frequencies of 1–100 kHz. The phase angle which optimally excluded a contribution from membrane conductance was selected by the method of Fidler and Fernandez (16) with series resistors of 20 kΩ at 100 kHz up to 200 kΩ at 1 kHz. Large membrane conductances could be activated—e.g., calcium-activated chloride current in oocyte patches—with no change of the monitored capacitance.

For higher time resolution, modified Axopatch 200A capacitance-feedback patch clamps were employed. A 2-MHz charge output and a 250-kHz current output were available. Data acquisition was performed at 8 MHz with 12-bit resolution, using custom hardware. For frequency scanning, the apparent capacitance was measured by the charge output as the signal component (i.e., charge moved) in phase with voltage. Changes of capacitance using an equivalent circuit resulted in constant capacitance changes over the entire frequency and voltage ranges employed.

Capacitance–voltage relations were determined with cumulative voltage step protocols using step durations of 2–50 ms. Frequency scanning was performed with a Hewlett–Packard 35665A dynamic signal analyzer. The highest frequencies presented are one-tenth the voltage clamp response rates demonstrated below. Model equations were fitted to data sets by a least-squares method.

Expression of Transporter Activities in *Xenopus* Oocytes. RNA (≈25 ng) encoding rat GAT1 transporter (13) was injected into *Xenopus* oocytes, and transporter currents and charge movements were recorded 3–5 days later in excised giant patches.

Experimental Solutions. For Na,K pump measurements, the pipette (extracellular) solution routinely contained 120 mM NaCl, 4 mM $MgCl_2$, 10 mM EGTA (with no added calcium),

The publication costs of this article were defrayed in part by page charge payment. This article must therefore be hereby marked "*advertisement*" in accordance with 18 U.S.C. §1734 solely to indicate this fact.

Abbreviations: GABA, γ-aminobutyric acid; DPA, dipicrylamine.
¶To whom reprint requests should be addressed.

and 10 mM Hepes. pH was adjusted to 7.0 with *N*-methylglucamine (NMG). The cytoplasmic solution was the same, except for a lower $MgCl_2$ concentration of 0.5 mM. NMG chloride was substituted for NaCl to vary the sodium concentration. Essentially the same solutions were used in the GAT1 capacitance measurements. NMG was substituted for sodium, and Mes (methanesulfonate) was substituted for chloride. When pipette chloride concentrations were less than 20 mM, an agar/0.3 M KCl bridge constructed from a 1.2-mm i.d. polyethylene tube, was used in the pipette.

Megahertz Voltage Clamp. Fig. 1 demonstrates the 1-MHz voltage clamp resolution achieved in giant membrane patches. The signals are charge records for voltage clamp of calcium-activated chloride current in an oocyte patch. Solutions on both membrane sides contain 100 mM CsCl. The pipette resistance was 50 kΩ, and the membrane capacitance was 5 pF. Charge signals were acquired in the absence and the presence of 2 μM free cytoplasmic calcium (10 mM EGTA/7 mM $CaCO_3$) to inhibit and activate, respectively, the chloride current. Fig. 1*A* shows a subtraction of charge signals in the absence of calcium from those in the presence of calcium. Since charge is the time integral of current, a horizontal line corresponds to zero current, a line with a positive slope is a steady outward current, and a line with a negative slope is a steady inward current. An exponential function plus a linear function was fitted to the data at each potential. The first derivative of the fitted function, which approximates membrane current, is shown in Fig. 1*B*. Time constants obtained at the onset of voltage steps were less than 0.5 μs.

RESULTS

Principle of Transporter Capacitance Measurements. Fig. 2 illustrates how a simple electrogenic reaction can be characterized by capacitance measurements. The figure shows the voltage and time dependencies of the apparent capacitance induced by the negatively charged hydrophobic ion DPA (17–19), applied at 0.2 μM to the cytoplasmic side of a cardiac membrane patch and with 1-mV voltage perturbations. The data points are subtractions of results in the absence of DPA from results in the presence of DPA. The membrane capacitance without DPA was constant over the entire voltage range monitored (see Fig. 4*E* for results from oocyte membrane).

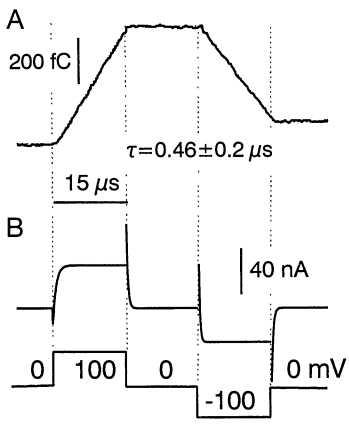

FIG. 1. A 1-MHz voltage clamp of calcium-activated chloride current in a giant *Xenopus* oocyte patch. Pipette resistance, 50 Ω; membrane capacitance, 5 pF; 100 mM CsCl on both sides. (*A*) Subtracted charge records or results with minus without 2 μM cytoplasmic free calcium. Voltage pulses were 15 μs. A fitted linear function plus an exponential corner function is plotted as a dotted line at each voltage with the data. The average time constant for adjustment of current to a new potential, τ, was 0.46 ± 0.2 μs (SEM, $n = 4$). (*B*) Membrane current, approximated as the first derivative of the functions fitted to the charge records.

Fig. 2*A* shows the voltage dependence of the DPA-induced capacitance. As illustrated, the hydrophobic anion resides primarily on the extracellular side at negative potentials and primarily on the cytoplasmic side at positive potentials. Accordingly, the DPA-induced capacitance, monitored by small voltage perturbations, is bell-shaped with a maximum at −10 mV. The fitted curve is proportional to the first derivative of the Boltzmann function, $1/\{1 + \exp[-\alpha(E_m - \beta)F/RT]\}$, with a slope parameter (α) of 0.76 and a midpoint (β) of −10 mV. These parameters are similar to those of others for DPA in natural membranes (18, 19). In oocyte membrane, the midpoint was more negative, −40 to −60 mV, suggesting that DPA tends to be excluded from the outer membrane leaflet. This might be caused, for example, by the glycosylation of extracellular lipids (see ref. 20 for review of membrane asymmetry).

Fig. 2*B* shows frequency spectra of the real and imaginary components of the DPA-induced signals. Equations describing the signals expected for a simple charge movement across a single barrier were derived (27) and fitted to the data points. The apparent DPA-induced capacitance, monitored as the real component of the charge signal (i.e., in phase with voltage) declines with increase of frequency according to the fitted equation $A/[1 + (f/f_c)^2]$, where f is frequency, f_c is the "corner" frequency, and A is a constant. The imaginary component of the charge signal (i.e., 90° out of phase from applied voltage) rises and falls according to the fitted equation $B{\cdot}f/[1 + (f/f_c)^2]$, where B is another constant.

The rate constant of the charge movement at 0 mV (i.e., the sum of forward and backward rate constants) corresponds to $1/(2\pi f_c)$, or 9500 s^{-1}. A slower component of DPA charge movements becomes evident at frequencies lower than shown here. The 9500 s^{-1} value is close to the rate obtained by voltage-step protocols in cardiac membrane (not shown), as well as to rates given for squid axon (18). The advantage of the capacitance method is its high sensitivity in spite of the small magnitude of voltage perturbations employed.

Capacitance Measurements of Na,K Pump Electrogenic Reactions. Capacitance changes which accompany conformational changes of the Na,K pump are presented in Fig. 3. The diagram in Fig. 3*A* depicts the major proposed Na,K pump states and their dependence on the major experimental variables (see open arrows). In the absence of cytoplasmic sodium and ATP, the pump is expected to orient with empty binding sites open to the cytoplasmic side ($E_1$0). Cytoplasmic sodium can bind to this enzyme form, giving rise to the $E_1$3N state, and the binding of one of the three sodium ions is suggested to be electrogenic on the basis of voltage-sensitive dye measurements with Na,K pump from other tissues and species (7, 21).

In 10 experiments, the cytoplasmic sodium concentration was varied from 0 to 20 mM, using various solution compositions without ATP. No changes of capacitance were found, suggesting that sodium binding from the cytoplasmic side is electroneutral in guinea-pig cardiac membrane.

When ATP is added in the presence of cytoplasmic sodium, the pump becomes phosphorylated with sodium occluded (the E_1P3N state). The pump can then open to the extracellular side to release sodium (reactions 3 and 4), giving rise to the E_2P3N and E_2P2N states. In the absence of extracellular potassium, the pump will accumulate in these E_2 states because reactions returning binding site availability to the cytoplasmic side with sodium bound instead of potassium (reactions 5 and 6) are very slow.

Fig. 3*B* shows typical capacitance changes observed during the application and removal of cytoplasmic sodium and ATP in the presence of 20 mM extracellular (pipette) sodium and 100 mM NMG (no other monovalent cation present). These records were obtained with a 30-kHz perturbation with 1-mV amplitude. Application of 10 mM sodium without ATP, or 1 mM ATP without sodium, results in no changes. The combined presence of cytoplasmic sodium (K_d, 4 mM) and ATP (K_d, 70

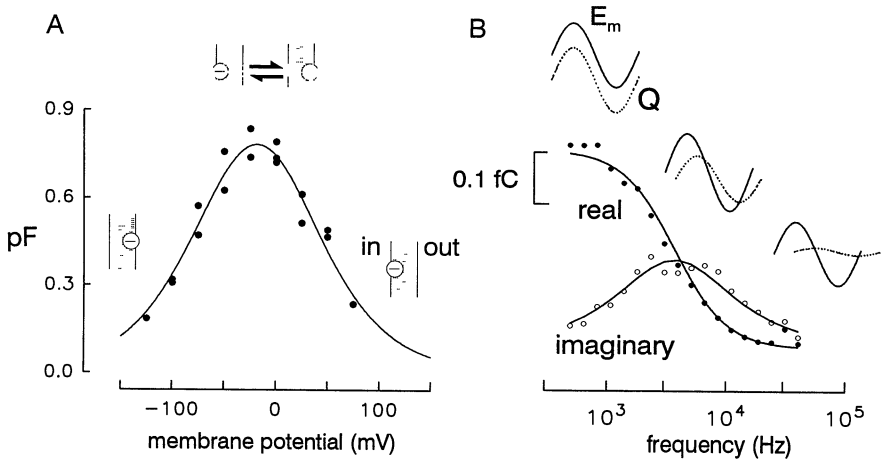

FIG. 2. Voltage and frequency dependence of the capacitance and admittance induced by a hydrophobic ion, dipicrylamine (DPA) (0.2 μM) in a cardiac myocyte patch. (*A*) Voltage dependence of DPA-induced capacitance. Results are the subtraction of capacitance–voltage relations obtained in control solutions from relations obtained with 0.2 μM DPA on the cytoplasmic side. (*B*) Frequency scan of the DPA-induced charge signal in 1-MHz voltage clamp. Capacitance is monitored as the "real" component of the charge signal (Q) in phase with applied voltage (E_m). The "imaginary" component, measured 90° from applied voltage, shows bell-shaped dependence on frequency. See text for description of data fits.

μM) induces a 180-fF increase of capacitance, which is immediately reversible on removal of either cytoplasmic sodium or ATP. The capacitance response amounts to about 2% of the total membrane capacitance.

Fig. 3*C* shows a frequency scan of the ATP-induced capacitance, measured at 38°C, in the presence of 100 mM cytoplasmic sodium. No response was obtained when 100 μM ouabain was included in the pipette. The pump-related capacitance declines from 0.75 pF at 50 Hz down to a steady value of 0.12 pF at 50 kHz. The spectrum is well described as the sum of two reactions, one "slow" charge-moving reaction with a corner frequency of 140 Hz (i.e., a rate constant of 880 s^{-1}), and one which is not resolved in this frequency range and therefore gives rise to a baseline capacitance, $A/[1 + (f/f_c)^2] + B$. These results are consistent with the Na,K pump charge movements described previously (9), whereby slow charge movements took place at 440 s^{-1} (0 mV, 35–37°C), and the magnitudes of fast components were about 1/10 the magnitudes of slow components.

The magnitudes of fast charge movements occurring in the E_2 pump configuration depend both on the extracellular sodium concentration and on membrane potential (9). High extracellular sodium and hyperpolarization shift the pump reactions toward the fully loaded, sodium-occluded state, manifested in a reduced capacitance (see open arrows in Fig. 3*A*). At very positive membrane potentials, most binding sites should be empty as the sodium release reactions are driven to completion.

Fig. 3*D* shows results for voltage steps from −100 mV to −50, 0, and +50 mV (1-mV perturbation at 100 kHz; 90 mM cytoplasmic sodium, 120 mM extracellular sodium, 32°C). As indicated, the results are shown in the absence of cytoplasmic ATP (−ATP) and in the presence of 1 mM ATP (+ATP). Capacitance signals settle within 50 μs in the absence of ATP, and they can be studied without background subtraction. Upon depolarization in the presence of cytoplasmic ATP, an immediate capacitance increase is followed by a slow rise of capacitance. Single exponential functions were fitted to the slow phase in each of the records, and the fitted functions are plotted as broken (barely visible) lines. The corresponding rate constants are plotted in Fig. 3*E* as a function of voltage.

In Fig. 3*F*, the steady-state capacitance is plotted as a function of voltage (typical for five similar experiments). Results are given for one patch with high (120 mM) extracellular sodium and another with low (20 mM) extracellular sodium. The capacitance–voltage relations in the absence of cytoplasmic ATP are typically flat (open triangles, from the experiment with 20 mM extracellular sodium). The solid lines

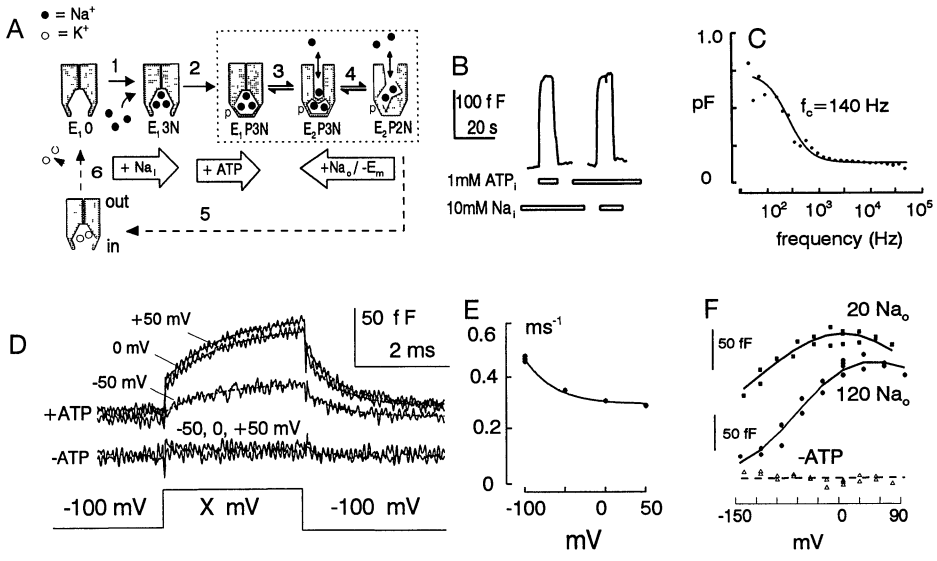

FIG. 3. Capacitance measurements of Na,K pump partial reactions in a giant cardiac-membrane patch. (*A*) State diagram of the Na,K pump cycle. Filled circles correspond to sodium ions and open circles to potassium ions. Open arrows indicate the influences of the major experimental variables. The major electrogenic reactions are thought to be fast sodium binding/unbinding reaction within the E_2P3N and the E_2P2N states (reaction 4). See text for further explanations. (*B*) Slow recordings of capacitance changes observed with combined application of sodium (10 mM) and ATP (1 mM) on the cytoplasmic side, and in the presence of extracellular sodium (20 mM). (*C*) Frequency scan of capacitance induced by 1 mM cytoplasmic ATP in the presence of 10 mM cytoplasmic sodium and 100 mM extracellular sodium. (*D*) High-speed capacitance signals during voltage pulses from −100 to −50, 0, or +50 mV (100 kHz, 0.5 mV perturbation; 20 mM cytoplasmic sodium; 120 mM extracellular sodium; 34°C). In the presence of 1 mM cytoplasmic Mg·ATP (+ATP), capacitance responds in a fast and slow phase. Broken lines with each record give single exponential functions fitted to the slow phases. (*E*) Voltage dependence of the rate constants from *C*. (*F*) Typical steady-state capacitance–voltage relations with low (20 mM) and high (120 mM) extracellular sodium. Results without ATP are from the patch with 20 mM extracellular sodium, using a slightly different voltage protocol. The solid lines in *E* and *F* are the predicted relations from a model used to simulate fast charge movements of the Na,K pump (8); results were scaled accordingly.

in Fig. 3 *E* and *F* are the predictions from a previously described model (9); the rate of the slow step (reaction 3) was decreased to account for these results at 32°C, and the simulated results were scaled to the experimental results in Fig. 3*F*. As predicted, the fast capacitance–voltage relation is bell-shaped, and it is shifted to more negative potentials at lower extracellular sodium concentrations.

We mention that we have similarly identified fast electrogenic reactions for the cardiac Na,Ca exchanger, expressed in *Xenopus* oocyte membrane (22, 23). Those results were also consistent with extracellular sodium binding being the major electrogenic reaction underlying capacitance signals. In contrast, the signals described below for the GAT1 transporter clearly have a different origin.

Capacitive Measurements of GAT1 (24) Charge-Moving Reactions. Fig. 4*A* shows a possible transport cycle for the GAT1 (GABA) transporter. It has been established that sodium can bind to the GAT1 transporter from the extracellular side in the absence of GABA and that this binding is followed by a large slow charge movement (ref. 13; reaction 1). Chloride is essential for the GAT1 transport cycle (25), and transport of chloride has been measured directly for the TAUT1 taurine transporter (D. D. F. Loo, K. K. Boorer, and E. M. Wright, personal communication). In addition, chloride may allosterically stimulate transport activity (26). It is established here, that in the absence of any bound substrate the carrier can reorient (reaction 2) to a configuration which allows cytoplasmic chloride to bind. The subsequent steps in a "reverse" cycle, including the binding and translocation of GABA and sodium (reactions 4 and 5), are not addressed by results to be presented. From the extracellular side it is known that chloride can bind to the transporter in the absence of GABA, and that GABA can bind without chloride (13). It is not known whether extracellular chloride can bind in the absence of extracellular sodium.

Addition of cytoplasmic chloride (100 mM) was found to decrease the membrane capacitance of GAT1-expressing patches in the absence of any other GAT1 substrates on either membrane side. Fig. 4*B* shows the chloride dependence of the capacitance decrease (closed circles); neither sodium nor GABA is present. The K_d is 15 mM. There is no change of membrane current (open circles) or conductance on application of cytoplasmic chloride.

Fig. 4*C* shows the cytoplasmic chloride dependence of both membrane capacitance and reverse transport current when 120 mM sodium and 2 mM GABA were included on the cytoplasmic side. The decrease of capacitance and the activation of reverse transport current show a very similar dependence on cytoplasmic chloride, suggesting a close relationship between these two events. Very similar results were obtained with extracellular chloride concentrations from 2 to 120 mM, strongly suggesting that extracellular chloride binding does not contribute significantly to the observed capacitance signals. A frequency scan of the capacitance decrease induced by 120 mM cytoplasmic chloride is shown in Fig. 4*D*; results without chloride were subtracted from results with chloride. The capacitance declines only slightly up to 20 kHz, indicating that the underlying charge-moving reaction is still faster.

As pointed out above, the GAT1 transporter can bind extracellular sodium and undergo a slow reaction which generates a large charge movement in the absence of other substrates. Therefore, we studied the relationship of the slow voltage-dependent step to the chloride-sensitive capacitance change. Fig. 4*E* shows the flat capacitance–voltage reactions obtained in control oocyte patches and the lack of effect of applying 120 mM chloride from the cytoplasmic side. As shown in Fig. 4*F*, membrane capacitance increased with depolarization in GAT1-containing patches when 120 mM sodium Mes was included in the pipette. Note that according to the model described, depolarization will drive the transporter from a configuration with occluded sodium ions to one in which the binding sites are empty (reaction 1). As further shown in Fig. 4*F*, addition of cytoplasmic chloride suppresses entirely the increase of capacitance with depolarization. This suggests, therefore, that both extracellular sodium and cytoplasmic chloride can suppress a charge-moving reaction of the transporter by occupying empty binding sites.

The time course of capacitance changes in the presence of 120 mM extracellular sodium was studied by using voltage steps over the range of −200 to +200 mV. As shown in Fig. 4*G*, capacitance increased with depolarization from −100 to +100 mV in a small fast phase and a more pronounced slow phase over a 50-ms step. Upon hyperpolarization, capacitance decreased in an immediate phase and a slow phase taking tens of milliseconds. In contrast, there was no slow phase in the presence of 120 mM cytoplasmic chloride. The slow capacitance changes were completely absent when the specific GABA transporter inhibitor SKF89976A (60 μM) was included in the pipette solution.

DISCUSSION

We have used capacitance measurements to identify two types of fast voltage-dependent interactions between ions and mem-

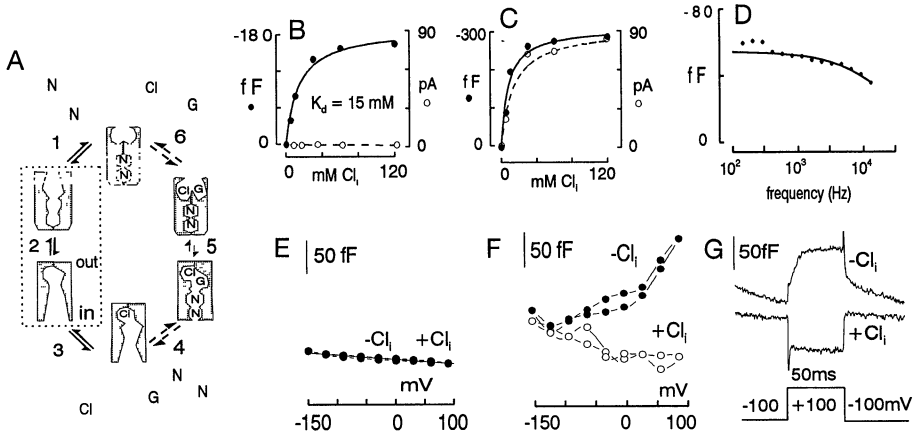

FIG. 4. Capacitance measurements of GAT1 electrogenic reactions in *Xenopus* oocyte patches. (*A*) Possible model of the GAT1 transport cycle, based on experimental results to date. See text for details. N, Na^+; G, GABA. (*B* and *C*) Concentration dependence of cytoplasmic chloride-induced reduction of capacitance of GAT1-containing patches, either in the absence (*B*) or in the presence (*C*) of 100 mM cytoplasmic sodium and 0.2 mM cytoplasmic GABA. In the latter case, an outward reverse transport current is induced upon addition of cytoplasmic chloride. The patches were held at 0 mV with 20 mM chloride on the extracellular (pipette) side. (*D*) Frequency scan of capacitance reduction induced by 100 mM cytoplasmic chloride, exchanged for 100 mM Mes. The line is the fitted function $-52\text{fF}/[1 + (f/29\text{ kHz})^2]$. (*E*) Typical capacitance–voltage relations of membrane patches from control oocytes in the presence and absence of 120 mM cytoplasmic chloride. (*F*) Typical capacitance–voltage relations from a GAT1-containing patch in the presence of 120 mM extracellular sodium. Note the voltage-dependent rise of capacitance and the suppression of this rise by cytoplasmic chloride. (*G*) Capacitance responses to step voltage changes in GAT1-containing patch with 120 mM extracellular sodium. Voltage was stepped from 0 to −100 mV 10 ms prior to the onset of signals.

brane transporters. Data for the Na,K pump indicate that the occupation of sodium binding sites per se is probably electrogenic, while results for the GAT1 cotransporter indicate that occupation of chloride binding sites can silence fast electrogenic reactions taking place in the absence of substrate. The validity of our approach is supported by analysis of a simple model system, the hydrophobic anion DPA.

The capacitance measurements for the Na,K pump confirm several expected behaviors (6, 7, 9). Membrane capacitance, monitored with up to 100-kHz perturbations, increases when the pump is phosphorylated. This increase of capacitance is dependent on extracellular sodium and membrane voltage, and the rate of capacitance change during voltage steps decreases monotonically with depolarization to about 300 s^{-1} at 32°C in Fig. 3*E*. This rate is strongly temperature sensitive, and a fitted value of 880 s^{-1} is obtained from the frequency scan at 38°C in Fig. 3*C*.

The model fitted to the results (9) assumes that the underlying slow process (reaction 3 in Fig. 3*A*) is a voltage-independent conformational change which opens sodium binding sites to the extracellular side. Accordingly, it could be analogous to a partial reaction of channel gating, and its strong temperature dependence indicates that it has a high activation energy. The Na,K pump results are all consistent with the idea that the increased capacitance of the pump with binding sites open to the extracellular side reflects binding of extracellular sodium by the pump. The actual capacitance may be generated by diffusion of sodium ions *per se*, if electrical field crosses through these binding sites, or it may be generated by fast conformational changes of the sodium binding sites as sodium binds.

The results for the GAT1 transporter document that the binding of cytoplasmic chloride ions silences a fast electrogenic reaction. The actual capacitance may be generated in this case by movements of charged groups of the empty binding sites within the membrane field. These movements may be associated with a transition between states, which allows alternatively extracellular sodium or cytoplasmic chloride to bind (reaction 2 of Fig. 4*A*). Our evidence that extracellular sodium also silences this fast reaction is indirect. In the presence of extracellular sodium the membrane capacitance rises in a time-dependent fashion as the membrane is depolarized. The slow kinetics of this reaction (Fig. 4*G*) correspond to the time course of a well-characterized slow charge movement of the transporter (13), whereby the binding sites are expected to be cleared of sodium at positive potentials. In the reaction scheme discussed (Fig. 4*A*), cytoplasmic chloride can logically suppress this increase of capacitance by drawing transporters into a configuration with binding sites open to the cytoplasmic side and occupied by chloride. The immediate jumps of capacitance on changing voltage, both in the case of the GAT1 transporter and in the case of the Na,K pump, logically reflect a nonlinearity of the capacitance resulting from fast electrogenic reactions. These reactions will saturate at extreme negative and positive potentials, albeit with less steep dependence on voltage than for results with DPA.

In conclusion, the present work documents the use of highly sensitive capacitance measurements in the study of electrogenic ion transporters. The ability to monitor partial transporter reactions related to ion binding should be useful, when combined with molecular biological and structural methods, in the development of structure–function models.

We thank Dr. H. Lester (California Institute of Technology) for helpful discussions, Dr. W. L. Hubbel (University of California, Los Angeles) for the generous gift of DPA, Dr. Rich Lobdill (Axon Instruments) for modifying the patch clamps employed, and Mr. Steve Callaway for technical assistance. This work was supported by Grant RO1 HL51323-02 from the National Institutes of Health and by a Grant-in-Aid from the American Heart Association.

1. Society of General Physiologists (1993) *Molecular Biology and Function of Carrier Proteins* (Rockefeller Univ. Press, New York), Vol. 48.
2. Deisenhofer, J., Epp, O., Miki, K., Huber, R. & Michel, H. (1985) *J. Mol. Biol.* **180,** 385–398.
3. Abrahams, J. P., Leslie, A. G. W., Lutter, R. & Walker, K. E. (1994) *Nature (London)* **370,** 621–631.
4. Läuger, P. (1991) *Electrogenic Ion Pumps* (Sinauer Associates, Sunderland, MA).
5. Klodos, I. & Forbush, B., III (1988) *J. Gen. Physiol.* **92,** 46a (abstr.).
6. Bühler, R., Stürmer, W., Apell, H. J. & Läuger, P. (1991) *J. Membr. Biol.* **121,** 141–161.
7. Heyse, S., Wuddel, I., Apell, H.-J. & Stürmer, W. (1994) *J. Gen. Physiol.* **104,** 197–240.
8. Gadsby, D. C., Rakowski, R. F. & De Weer, P. (1993) *Science* **260,** 100–103.
9. Hilgemann, D. W. (1994) *Science* **263,** 1429–1432.
10. Lagnado, L., Cervetto, L. & McNaughton, P. A. (1988) *Proc. Natl. Acad. Sci. USA* **85,** 4548–4552.
11. Loo, D. D., Hazama, A., Supplisson, S., Turk, E. & Wright, E. M. (1993) *Proc. Natl. Acad. Sci. USA* **90,** 5767–5772.
12. Hilgemann, D. W., Nicoll, D. A. & Philipson, K. D. (1991) *Nature (London)* **352,** 715–718.
13. Mager, S., Naeve, J., Quick, M., Labarca, C., Davidson, N. & Lester, H. A. (1993) *Neuron* **10,** 177–188.
14. Collins, A., Somlyo, A. V. & Hilgemann, D. W. (1992) *J. Physiol. (London)* **454,** 27–57.
15. Hilgemann, D. W. (1995) in *Single Channel Recording*, eds. Sakmann, B. & Neher, E. (Plenum, New York), 2nd Ed., pp. 307–326.
16. Fidler, J. & Fernandez, J. (1989) *Biophys. J.* **56,** 1153–1162.
17. Benz, R. & Läuger, P. (1977) *Biochim. Biophys. Acta* **468,** 245–258.
18. Benz, R. & Nonner, W. (1981) *J. Membr. Biol.* **59,** 127–134.
19. Fernandez, J. M., Taylor, R. E. & Bezanilla, F. (1983) *J. Gen. Physiol.* **82,** 331–346.
20. Mato, J. M. (1990) *Phospholipid Metabolism in Cellular Signaling* (CRC, Boca Raton, FL).
21. Schwappanch, B., Stuermer, W., Apell, H. J. & Karlish, S. J. (1994) *J. Biol. Chem.* **269,** 21620–21626.
22. Hilgemann, D. W. (1995) *Heart Vessels Suppl.* **9,** 155–158.
23. Hilgemann, D. W. (1995) in *Cardiac Sodium-Calcium Exchange*, Proceedings of the Third International Meeting (New York Acad. of Sci., New York), in press.
24. Guastella, J. G., Nelson, N., Nelson, H., Czyzyk, L., Keynan, S., Midel, M. C., Davidson, N., Lester, H. & Kanner, B. (1990) *Science* **249,** 1303–1306.
25. Kanner, B. I. & Schuldiner, S. (1987) *CRC Crit. Rev.* **22,** 1–38.
26. Cammack, J. N., Rakhilin, S. V. & Schwarz, E. (1994) *Neuron* **13,** 949–960.
27. Markin, V. S., Pastushenko, V. F. & Chizmadzhev, Y. A. (1987) *Theory of Excitable Media* (Wiley, New York).